Journal of the Ceramic Society of Japan 125 [7] 552-558 2017 Special Article
The 71st CerSJ Awards for Advancements in Ceramic Science and Technology: Review

Low-temperature synthesis and rational design of nitrides and oxynitrides for novel functional material development

Akira MIURA†

Faculty of Engineering, Hokkaido University, Kita 13, Nishi 8, Kita-ku, Sapporo 060–8628, Japan

Nitrides and oxynitrides exhibit great potential for novel material development, since their electronic structures can be controlled by tuning the amounts of air-abundant nitrogen and oxygen elements therein. However, the above control methods still need to be developed, and the crystal and electronic structures of the produced nitrides/oxynitrides need to be understood. Herein, I summarize the recent progress in nitride and oxynitride synthesis, highlighting novel low-temperature nitridation of oxides by molten $NaNH_2$, and attempt to rationalize the crystal and electronic structures of nitride and oxynitrides. Moreover, I describe how the catalytic activity of manganese oxynitrides in the oxygen reduction reaction can be enhanced by tuning their nitrogen content and thus their electronic structures.

Key-words : $NaNH_2$, DFT calculation, Crystal structure, Electronic structure, X-ray diffraction, Oxygen reduction reaction

[Received March 19, 2017; Accepted May 13, 2017]

1. Introduction: background and challenges of nitrides and oxynitrides

Most traditional and novel ceramics are based on oxides with oxygen anion (O^{2-}) since oxides are often thermodynamically stable and can be synthesized by high-temperature heating in air. Meanwhile, nitrides and oxynitrides contain nitrogen anion (N^{3-}), of which ion radius (1.46 Å[1]) is close to that of oxygen anion (1.38 Å[1]). Thus, nitrides and oxynitrides may be viewed as a simple extension of oxides, with oxygen anions (partially) substituted by nitrogen anions. It follows that the electronic structures of nitrides and oxynitrides can be modified by tuning the contents of oxygen/nitrogen anions, with the resulting variety of electronic structures being advantageous for fabricating functional materials such as blue light-emitting diodes based on GaN and (Ga,In)N,[2),3)] superconductors based on NbN and ZrNCl,[4)–6)] SiAlON-based refractory materials and phosphors,[7),8)] optically active materials including pigments, UV absorbers, and photocatalysts,[9)–12)] and ferromagnetic materials.[13),14)] However, the number of materials based on nitrides and oxynitrides is still much less than that of their oxide-based counterparts.

Nitrides are less thermodynamically stable than oxides due to the high stability of molecular nitrogen, which contains a triple bond.[15)] Therefore, high-temperature heating of nitrides under ambient pressure often results in either partial or total loss of nitrogen anions due to the entropy increase associated with the formation of N_2 gas[15)] [Eqs. (1) and (2)].

$$MN \rightarrow M + 0.5N_2 \quad \text{(M: metal)} \quad (1)$$

$$MN \rightarrow MN_{0.5} + 0.25N_2 \quad (2)$$

The triple bond in molecular nitrogen (941 kJ/mol) is much stronger than the double bond in molecular oxygen (500 kJ/mol), accounting for lower formation energies of nitrides compared to those of oxides.[15)] As a result, the formation of an oxide and a nitrogen molecule is more thermodynamically favorable than that of a nitride and an oxygen molecule [Eq. (3)].

$$MN + 0.5O_2 \rightarrow MO + 0.5N_2 \quad (3)$$

Hence, nitridation of oxides cannot be achieved by thermal treatment in an atmosphere of air or nitrogen. However, oxides can be converted to nitrides or oxynitrides by heating in a flow of ammonia, which is thermodynamically driven by the formation of water [ΔG_f (H_2O) = −228.6 kJ/mol[16)]] from ammonia gas [$\Delta G_f(NH_3) = -16.4$ kJ/mol[16)]] [Eq. (4)]. Moreover, water is purged from the reaction system by the ammonia flow, making the formation of nitrides even more preferable. Accordingly, this approach utilizes large amounts of ammonia gas.

$$MO + 0.5NH_3 \rightarrow MN + H_2O + 0.5H_2 \quad (4)$$

Figure 1 shows typical synthesis methods of nitride and oxynitride categorized according to their pressure and temperature requirements. High pressure of nitrogen gas shifts the equilibriums presented in Eqs. (1) and (2) to the left. Thus, high pressure is useful to stabilize nitrogen anions even in high temperature. From

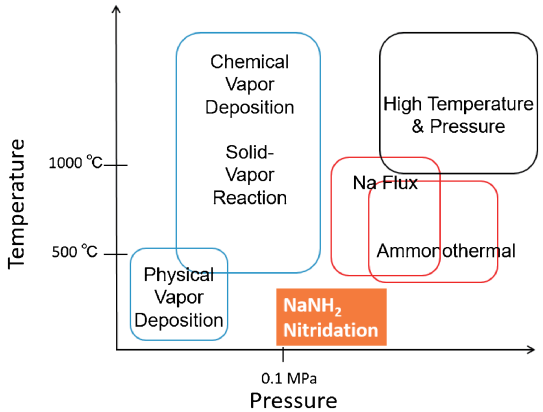

Fig. 1. Typical conditions of nitride/oxynitride synthesis.

† Corresponding author: A. Miura; E-mail: amiura@eng.hokudai.ac.jp

DOI http://doi.org/10.2109/jcersj2.17055

the kinetic point of view, high temperature results in fast diffusion of oxygen and nitrogen anions to form nitrides/oxynitrides. Hence, high-temperature and high-pressure method is attractive for the synthesis of nitrides and oxynitrides.[17)–22)] However, this approach is energy-consuming and requires specialized reactors. Multi-anvil presses can be used to explore high-pressure chemistry, but produces a rather small amount of products.

Although low temperatures stabilize nitrogen anions in nitrides/oxynitrides, they often limit nitridation rates. Thus, the use of solution- or vapor-phase processes is required to enhance reaction kinetics, as exemplified by Na flux[23)–25)] and ammonothermal methods,[26),27)] which allow nitrides/oxynitrides to be successfully synthesized at moderate temperatures and pressures. Moreover, these processes can afford metastable phases and are useful for preparing powders and bulk single crystals.

Vapor-phase reactions, e.g., chemical vapor deposition and vapor–solid reactions, can produce a range of nitrides and oxynitrides with various phases and morphologies. For instance, the heating of silicon/gallium oxides with carbon in a flow of nitrogen/ammonia forms the corresponding nitrides.[28)–33)] In these reactions, carbothermal reduction results in CO gas evolution, with N_2/NH_3 acting as nitridation agents. Nitrides and oxynitrides are prepared by heating oxides in a flow of NH_3 at a controlled heating temperature for a certain time.[34)–41)] The flow rate of ammonia gas is also important to control the partial pressures of ammonia, intermediates (e.g., NH_2 and NH[42)]), and the H_2O byproduct.[43),44)] However, these vapor-phase reactions often require moderate temperatures and large amounts of ammonia gas. Physical vapor deposition (PVD) techniques include sputtering and pulsed laser deposition,[45),46)] enabling the fabrication of thin films at low temperatures. Recently, nitrides have been rapidly synthesized at room temperature by reacting oxides with N_2 plasma.[47)] However, large-scale PVD-based synthesis is challenging, commonly requiring high-vacuum conditions.

In order to control composition and structure of oxynitrides/nitrides, the decrease in synthesis temperature would be attractive. Low-temperature approaches for the synthesis of nitride nanoparticle involve the reactions with halides with $NaNH_2$, NaN_3, Li_3N and $LiNH_2$[48)–55)] Very recently, a perovskite oxynitride, $BaTaO_2N$, is synthesized from $Ba(OH)_2$, $TaCl_5$ and $NaNH_2$ at 220°C, which is significantly lower than the reported method using oxides and NH_3 gas.[56)] Another alternative approach features the thermal decomposition of complexes containing NH_2^- or N^{3-}.[57),58)] Microwave reactions are also reported, which lower the required reaction temperature and/or time.[43),44)] Low-temperature synthesis exhibits the additional advantage of producing metastable phases. For example, $AgTaN_2$, in which linear N–Ag–N bonding with antibonding states exist below the Fermi level, can be synthesized by a topotactic reaction between $NaTaN_2$ and $AgNO_3$ at ~200°C.[59),60)]

Other challenging issues are of theoretical nature, e.g., the role of nitrogen content in controlling crystal and electronic structures. Assuming that the crystal structure of a given oxide does not change after substituting oxygen anions with nitrogen anions, the following electronic structure changes are expected.

(i) Anions are the major contributors to the top valence band levels of semiconductors. Thus, the introduction of nitrogen reduces the corresponding band gap, since the energy state of nitrogen is higher than that of oxygen.[61)]

(ii) Since nitrogen-metal bonds exhibit more covalent character than metal-oxygen ones,[61)] the conduction band of nitrides/oxynitrides is more dispersed, and their electron mobility is increased.

(iii) Nitrogen has fewer electrons than oxygen, which generally reduces the energy of the Fermi level and increases cation valences.

In practice, however, the incorporation of nitrogen anions often significantly changes the coordination of cations, thus altering the corresponding crystal structures. Hence, analysis of simple structures, e.g., NaCl-type ones, is essential for understanding how nitrogen anions affect chemical bonding and electronic structures. Moreover, the development of (oxy)nitride design principles based on the control of chemical bonding and electronic structure is highly desirable to create new functional materials.

In this review, I introduce the recent advances in low-temperature syntheses of nitrides and oxynitrides, highlighting a novel method utilizing molten $NaNH_2$, and rationalize NaCl-type structures of oxides, nitrides, and carbides. In addition, I describe the enhanced catalytic activities of nitrogen-rich manganese oxynitrides as an example of successful material design based on electronic structure and property tuning.

2. Low-temperature nitridation of oxides using $NaNH_2$

Although nitridation of oxides is often performed at high or moderate temperatures in a flow of ammonia or nitrogen, low-temperature nitridation has the potential to produce nitrides/oxynitrides with controlled morphologies and compositions, which may not be obtained by high or moderate temperatures. However, this low-temperature process involves the cleavage of strong metal-oxygen bonds and requires formation of metal-nitrogen bonds at an acceptable rate even at low temperature. Recently, our group have developed a new nitridation process based on the use of $NaNH_2$, which is commercially available, relatively inexpensive (~10,000 JPY/kg), and has a suitably low melting point (~210°C). Although $NaNH_2$ has been previously used for the nitridation of metals and oxides, this process requires temperatures above 500°C.[62)–66)] Conversely, our novel method allows low-temperature nitridation, using solid oxide/sodium amide powder mixtures in a closed system, with reaction control achieved without relying on a flow of ammonia.

The above nitridation is performed in three steps. First, oxide powders loaded into a steel crucible together with excess $NaNH_2$ are placed in an Ar- or N_2-filled glove box. Second, the crucible is heated in a closed system, typically in an autoclave, which can be Teflon-lined for reactions below ~260°C. After heating, excess $NaNH_2$ and the NaOH byproduct are removed using ethanol or ethanol/water, and the obtained product is dried. This approach allows successful nitridation of iron, manganese, copper, and indium oxides below 300°C (**Fig. 2**).[67)–70)] Notably, $NaNH_2$ reacts violently with water, requiring careful handling.

Figure 3 shows SEM images of $Fe_{3-x}N$ particles after nitridation.[68)] Low-magnification SEM images show that the particle shape does not significantly change after heating, whereas high-magnification SEM images show the presence of smaller particles, attributed to the decrease in the number of anions by the replacement of oxygen anions by less nitrogen anions. Nitridation of manganese and copper oxides was similar to that of iron oxides, i.e., low-magnification SEM images indicated unchanged morphologies, with high-magnification SEM images detecting the presence of smaller particles.[68),69)] As expected, the surface of the produced nitrides was covered with oxides and/or hydroxides, as shown in Eq. (3).[68)] On the other hand, nitridation of irregularly-shaped $LiInO_2$ produced hexagonal InN crystals (**Fig. 4**),[67)] suggesting a dissolution-reprecipitation mechanism of InN crystal

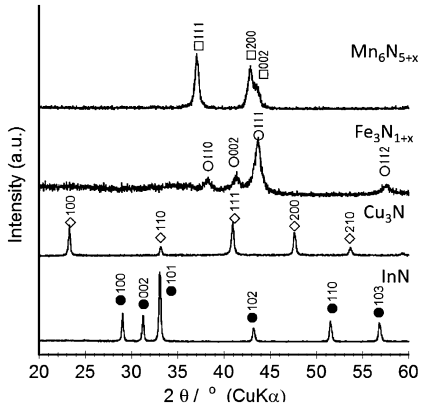

Fig. 2. XRD patterns of nitrides obtained using the low-temperature $NaNH_2$ method.

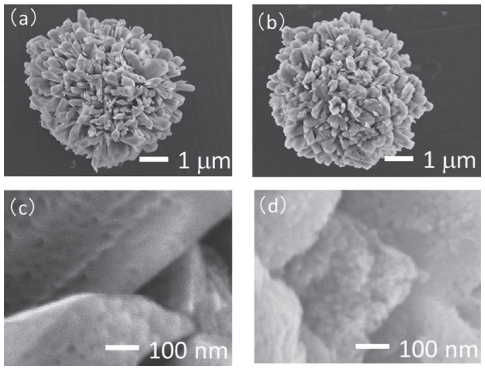

Fig. 3. Low-magnification scanning electron microscopy (SEM) images of Fe_2O_3 powder (a) before and (b) after nitridation, with the corresponding high-magnification SEM images shown in (c) and (d), respectively. Reprinted with permission from *Inorg. Chem.*, **52**, 11787–11791 (2013). Copyright 2013 American Chemical Society.

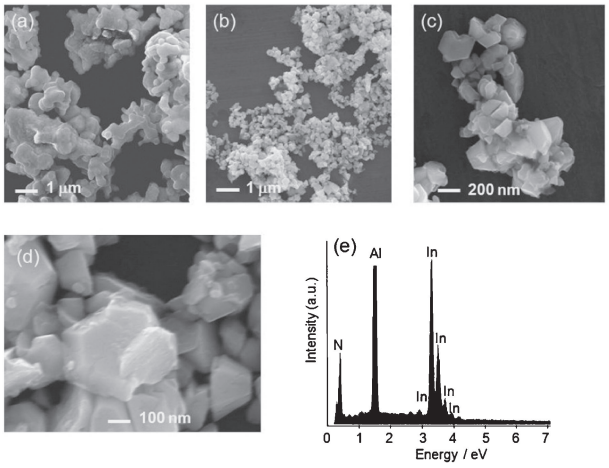

Fig. 4. SEM images of (a) $LiInO_2$ and (b–d) InN crystals at different magnifications (10–100 k). (e) Typical energy-dispersive X-ray spectrum of InN crystals. Reprinted with permission from *Cryst. Growth Des.*, **12**, 4545–4547 (2012). Copyright 2012 American Chemical Society.

growth. The addition of Teflon pieces enhanced the kinetics of $LiInO_2$ nitridation, presumably via formation of intermediates.[70]

Nitridation by $NaNH_2$ is thermodynamically driven by the formation of NaOH as a byproduct, as exemplified by the case of Fe_2O_3.[68]

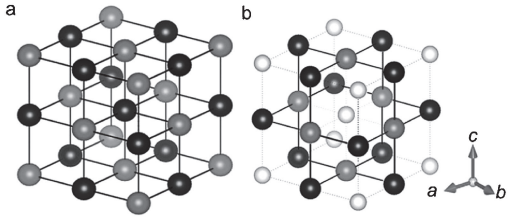

Fig. 5. Crystal structures of (a) sixfold-coordinated NbC and NbN and (b) fourfold-coordinated NbO. Dark and light grey spheres represent Nb and C/N/O, respectively. White spheres represent ordered vacancies. Reprinted with permission from *Inorg. Chem.*, **52**, 9699–9701 (2013). Copyright 2013 American Chemical Society.

$$1.5Fe_2O_3 + 4.5NaNH_2 \rightarrow Fe_3N + 4.5NaOH + N_2 + 1.5NH_3 \quad (5)$$

As described above, the strong triple bond in molecular nitrogen destabilizes nitrides with respect to oxides in terms of Gibbs free energy of formation (Fe_3N: $-30\,kJ/mol$;[71),72)] Fe_2O_3: $-744.8\,kJ/mol$[16)]). However, this reaction [Eq. (5)] is driven by large formation energy of a sodium hydroxide byproduct (NaOH: $-379.49\,kJ/mol$[16)]), with the change in the Gibbs free energy equaling $-269\,kJ/mol$.[68)] Moreover, the concentration of NH_2 in molten $NaNH_2$ is ~500 times higher than that of NH_3 in commonly used NH_3 gas, enhancing nitridation. Additionally, the single N–H bonds of sodium amide are better suited for nitride formation than the triple bond of N_2. Although the reactivity of $NaNH_2$ toward oxygen and moisture necessitates handling it in an atmosphere of dry Ar or N_2, $NaNH_2$ is thus useful as a nitrogen source for low-temperature nitridation.

3. Chemical bonding and crystal structures of NaCl-type carbide, nitrides and oxides

NaCl-type structures can be used as a simple model to examine how nitrogen anions affect chemical bonding and structures.[73)] Niobium carbide, nitride, and monoxide exhibit NaCl-type structures, being formally described as NbX (X = C, N, O). NbC and NbN adopt a sixfold-coordinated structure,[74),75)] whereas NbO adopts a fourfold-coordinated structure, with a quarter of the vacancies present at both Nb and O sites (**Fig. 5**).[76)] The unique structure of NbO cannot be explained using a simple ionic model.[77)] Experimentally obtained structures of NbC and NbN presumably contain vacancies, but there are e no reports regarding the vacancies at both Nb and X sites in these species.

Figure 6 shows the calculated bond lengths and formation energies of NbX, assuming that the same proportion of Nb and X sites form vacancies in each species. Specifically, vacancy-free NbX forms a sixfold-coordinated NaCl structure, and NbX containing 25% vacancies forms a fourfold-coordinated NbO structure.[73)] The plot of bond length vs. vacancy concentration (0–25%) exhibits the largest slope in the case of NbO, followed by NbN, with the least value observed for NbC. Thus, increasing the atomic number of X tends to increase the rate of bond shortening upon vacancy introduction. Although the formation of these vacancies destabilizes NbC, it stabilizes NbO. Up to a vacancy content of 12.5%, the formation energies hardly change in NbN, indicating that the introduction of vacancies into NbN is not thermodynamically difficult.

Figure 7 shows the electron densities of NbX derived from synchrotron X-ray diffraction data, revealing that the orbitals in fourfold-coordinated NbO are more hybridized than those in sixfold-coordinated NbC.[73)] Hence, bonding in NbO is more

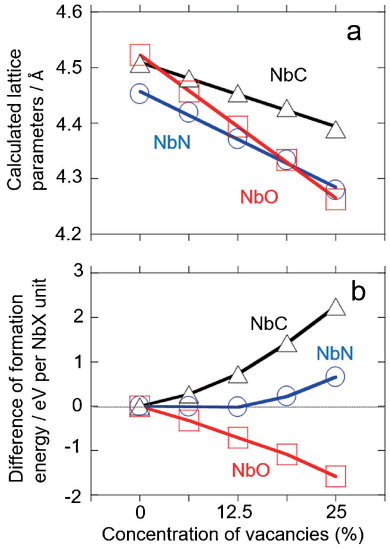

Fig. 6. (a) Average Nb–X bond lengths and (b) formation energy differences of NaCl-type NbX (X = C, N, O) with vacancy concentrations between 0 and 25% and the same number of Nb and X atoms. Data were calculated using the Vienna Ab initio simulation package (VASP). Zero energy was assigned to six-fold-coordinated NaCl structures and is indicated by a dotted line. Reprinted with permission from *Inorg. Chem.*, **52**, 9699–9701 (2013). Copyright 2013 American Chemical Society.

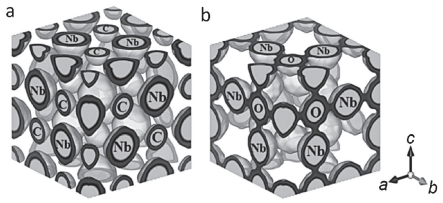

Fig. 7. Three-dimensional room-temperature electron density distributions of (a) NbC and (b) NbO determined based on synchrotron X-ray diffraction data using the maximum entropy method, showing an equidensity surface level of 0.85 eÅ^{-3}. Reprinted with permission from *Inorg. Chem.*, **52**, 9699–9701 (2013). Copyright 2013 American Chemical Society.

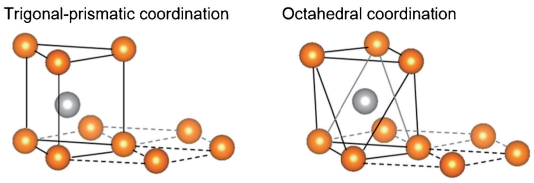

Fig. 8. Schematic diagrams of trigonal prismatic and octahedral coordination. Reprinted with permission from *J. Solid State Chem.*, **229**, 272–277 (2015). Copyright 2015 Elsevier.

covalent in character than that in NbC. Greater hybridization in NbO than that in NbC is supported by crystal orbital Hamilton population analyses based on theoretical data,[78] which suggests that although Nb–Nb interactions significantly affect the crystal structure, the contribution of Nb–Nb bonding is less significant than that of Nb–X bonding. Hence, increasing the atomic number of X from C to O results in increased hybridization and reduced Nb–X bond length and coordination number.

Two-dimensionally layered NaCl-type oxides/nitrides often adopt sixfold-coordinated structures with either octahedral or trigonal prismatic coordination (**Fig. 8**). For example, $NaNbN_2$

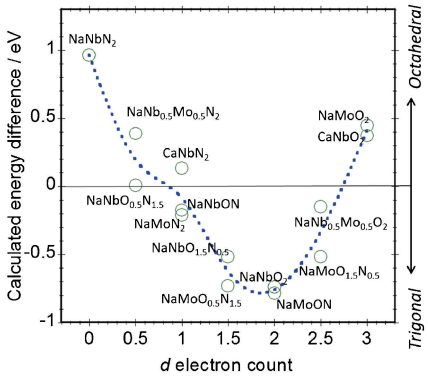

Fig. 9. Formation energy differences of various ABX_2 oxides, nitrides and oxynitrides isostructural with $NaNbN_2$ (octahedral) and $NaNbO_2$ (trigonal prismatic), calculated using VASP. Charge transfer from alkali/alkali earth metals and O^{2-}/N^{3-} ions to Nb/Mo was assumed to be equivalent to *d*-electron counts. Some of these compounds are hypothetical and have not been experimentally reported. The dashed line is provided as an eye guide. Reprinted with permission from *J. Solid State Chem.*, **229**, 272–277 (2015). Copyright 2015 Elsevier.

consists of alternating Na–N_6 and Nb–N_6 octahedra,[63] whereas $NaNbO_2$ features alternating Na–O_6 octahedra and Nb–O_6 trigonal prisms.[79] Structural differences between octahedral and trigonal prismatic coordination have been theoretically studied for layered sulfides and selenides by Kertesz and Hoffmann,[80] who showed that the count of *d* electrons and interactions of *d*-orbitals are key factors influencing these structural changes. Thus, layered ABX_2 oxides/oxynitrides/nitrides need to be further investigated to develop and characterize related materials.

Figure 9 shows the energy differences between trigonal prismatic and octahedral coordination of layered Nb and Mo oxides/oxynitrides/nitrides in terms of *d*-electron counts based on density functional theory (DFT) calculations, revealing that electron counts of 1–2.4 favor trigonal prismatic coordination, with other counts (up to a maximum of 3) favoring octahedral coordination.[81] Trigonal prismatic coordination increases the hybridization of *d*-orbitals, stabilizing the corresponding structures formed by non-closed-packed anions, which can be experimentally visualized using XRD-derived electron density data.[81] The experimentally obtained structures of Nb-, Mo-, Ta-, and W-based layered oxides/oxynitrides/nitrides agree with the electron count results.[81] Furthermore, structures containing 3*d*- and 4*d*-metals, e.g., Fe_xWN_2,[82–86] $MnMoN_2$,[82] $AgTaN_2$,[59,60] $CuNbN_2$,[87,88] and $CuTaN_2$,[89] can be rationalized in the same manner, assuming that Cu^+ and Ag^+ are monovalent and Fe^{2+} and Mn^{2+} are divalent.

4. Correlation between electronic structure and catalytic activity of manganese oxynitrides in the oxygen reduction reaction (ORR)

In this section, I introduce an example showing the relationships between nitrogen/oxygen content, electronic structure, and functionality of oxynitrides, providing helpful insights to facilitate the development and design of novel oxynitride materials.[90] Catalysts for the ORR in alkaline solution ($O_2 + 2H_2O + 4e^- \rightarrow 4OH^-$) have been extensively studied, being key materials for the production of fuel cells and metal-oxygen batteries. Although (oxy)nitride ORR catalysts have been recently reported,[91–95] the corresponding catalytic mechanism and design principles have not been fully characterized, in contrast to those of oxide catalysts. For instance, the correlation between electronic structures

Table 1. Structural properties of manganese oxynitrides.[90] Reprinted with permission from *Angew. Chem. Int. Ed. Engl.*, **55**, 7963–7967 (2016). Copyright 2016 Wiley

	MnON(1)	MnON(2)	MnON(3)
Mn:O:N molar ratio[a]	1:0.24:0.84	1:0.19:0.78	1:0.19:0.64
$Mn_4(O,N)_4$ cell/nm	$a = 0.421673(14)$	$a = 0.420866(16)$	$a = 0.420530(10)$
	$c = 0.414716(14)$	$c = 0.410434(16)$	$c = 0.405067(13)$
Occupancy of (O,N) site[b]	0.998(6)	0.889(9)	0.779(1)
Mn valence[c]	3.0	2.8	2.4

[a] Combustion analysis; calculated from measured values for N and O, and residuals for Mn.
[b] Derived from Rietveld analysis, assuming that anion sites are occupied only by nitrogen and that cation sites are fully occupied by manganese.
[c] Estimated values from Mn *K*-edge X-ray absorption.

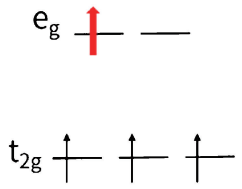

Fig. 10. High-spin configuration of octahedral Mn^{3+}–$(O,N)_6$.

and ORR activity has been studied for perovskite-structured $LaMO_3$ compounds (M = 3*d*-metal).[96)–101)] Perovskite oxides comprise metal-oxygen octahedra, the electronic structures of which can be described in terms of t_g and e_g states. Suntivich et al. have reported that close-to-single-electron occupancy of e_g states, e.g., in $LaMnO_3$, favors electron transfer during the ORR cycle.[101)] Oxides, oxynitrides and nitrides with NaCl-type structures are similar to perovskite oxides in terms of metal-anion octahedra and electronic structures, i.e., both MnO and MnN_x ($x \geq 2/3$) adopt NaCl-type structures comprising metal-oxygen/nitrogen octahedra.[102)] Moreover, stoichiometric MnN theoretically possesses a single electron in the e_g state, similarly to $LaMnO_3$ (Mn^{3+}; **Fig. 10**). Therefore, manganese oxynitrides with different N/O contents are suitable octahedral models for examining the effect of nitrogen on ORR activity.[90)]

Three manganese oxynitrides with different nitrogen contents synthesized by reacting manganese oxides with $NaNH_2$ were characterized by O/N combustion analysis and X-ray diffraction/absorption, with their catalytic activities evaluated in the ORR reaction. The above analyses showed that increased nitrogen content reduced the number of anion site vacancies and increased the lattice parameters of NaCl-type structures (**Table 1**),[90)] also increasing the valence of manganese and enhancing ORR catalytic activity (**Fig. 11**). The increased ORR catalytic activity was explained by close-to-single-electron occupancy of e_g states, similarly to the case of perovskite oxides.[90)] Furthermore, the greater covalent character of Mn–N bonding may also improve catalytic activity due to enhanced electron mobility and increased energies of e_g states.[90)] Overall, the obtained results suggest that tuning the electronic structures of oxynitrides by changing their N/O contents is a useful general strategy for developing novel functional materials.

5. Summary

Although nitrides and oxynitrides are promising compounds for the development of novel functional materials, exhibiting electronic structures that can be tuned by N/O content adjustment, their synthesis and property rationalization remain challenging. In this review, I describe a recently developed method for low-temperature (oxy)nitride synthesis using molten $NaNH_2$ and oxides as starting materials. The above protocol allows one to prepare nitrides and oxynitrides that may not be obtained using high-temperature approaches. Structural analyses of NaCl-type structures based on XRD and DFT characterizations reveal the relationships of chemical bonding and crystal/electronic structures of carbides, nitrides, and oxides. Moreover, I propose an ORR oxynitride catalyst design principle similar to that used for oxides, suggesting that oxynitrides can potentially exhibit greater catalytic activities due to their favorable electronic structures and high metal-nitrogen bond covalency. I believe that new synthesis methods and design principles can bridge the gap between oxide and nitride chemistry and contribute to the development of novel functional nitrides and oxynitrides.

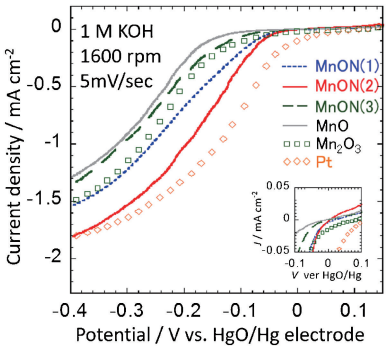

Fig. 11. Linear sweep polarization curves of MnON(1), MnON(2), MnON(3), and MnO obtained using a rotating disc electrode in O_2-saturated 1 M KOH at a sweep rate of 5 mV s^{-1}.[90)] Reprinted with permission from *Angew. Chem. Int. Ed. Engl.*, **55**, 7963–7967 (2016). Copyright 2016 Wiley.

Acknowledgements In acknowledging the contributions of numerous co-researchers, I wish to express my particular gratitude to Prof. Kiyoharu Tadanaga, Prof. Mikio Higuchi, Prof. Carolina Rosero and Prof. Yuji Masubuchi at Hokkaido University, Prof. Nobuhiro Kumada and Prof. Takahiro Takei at University of Yamanashi, and Prof. Eisuke Magome, Prof. Chikako Moriyoshi, and Prof. Yoshihiro Kuroiwa at Hiroshima University. I wish to acknowledge Prof. Francis J. DiSalvo at Cornell University and Prof. Richard Dronskowski at RTWH Aachen University. I express sincere thanks to Prof. Shiro Shimada and Prof. Shinichi Kikkawa, who guide me in this field. This research was partially supported by a JSPS Grant-in-Aid for Young Scientists (No. 25820330 and 17H04950).

References

1) R. D. Shannon, *Acta Crystallogr. A*, 32, 751–767 (1976).
2) H. Amano, M. Kito, K. Hiramatsu and I. Akasaki, *Jpn. J. Appl. Phys.*, 28, L2112–L2114 (1989).

3) I. Akasaki, *Angew. Chem., Int. Ed.*, **54**, 7750–7763 (2015).
4) T. Mitszuoka, T. Yamashita, T. Nakazawa, Y. Onodera, Y. Saito and T. Anayama, *J. Appl. Phys.*, **39**, 4788–4791 (1968).
5) Y. Ohashi, Y. Masubuchi, D. Venkateshwarlu, V. Ganesan, J. V. Yakhmi, T. Yoshida and S. Kikkawa, *J. Solid State Chem.*, **210**, 238–241 (2014).
6) S. Yamanaka, H. Kawaji, K.-i. Hotehama and M. Ohashi, *Adv. Mater.*, **8**, 771–774 (1996).
7) Y. Oyama and O. Kamigaito, *Jpn. J. Appl. Phys.*, **10**, 1637 (1971).
8) K. Uheda, N. Hirosaki and H. Yamamoto, *Phys. Status. Solidi A*, **203**, 2712–2717 (2006).
9) K. Maeda, T. Takata, M. Hara, N. Saito, Y. Inoue, H. Kobayashi and K. Domen, *J. Am. Chem. Soc.*, **127**, 8286–8287 (2005).
10) F. Tessier, P. Maillard, F. Cheviré, K. Domen and S. Kikkawa, *J. Ceram. Soc. Jpn.*, **117**, 1–5 (2009).
11) M. Jansen and H. P. Letschert, *Nature*, **404**, 980–982 (2000).
12) M. Yashima, H. Yamada, K. Maeda and K. Domen, *Chem. Commun.*, **46**, 2379–2381 (2010).
13) S. Yamashita, Y. Masubuchi, Y. Nakazawa, T. Okayama, M. Tsuchiya and S. Kikkawa, *J. Solid State Chem.*, **194**, 76–79 (2012).
14) S. Bhattacharyya, *J. Phys. Chem. C*, **119**, 1601–1622 (2015).
15) F. J. DiSalvo and S. J. Clarke, *Curr. Opin. Solid State Mater. Sci.*, **1**, 241–249 (1996).
16) CRC Handbook of Chemistry and Physics, 83rd Edition, CRC Press, Boca Raton, Fulorida (2002).
17) S. Porowski and I. Grzegory, *J. Cryst. Growth*, **178**, 174–188 (1997).
18) M. Wessel and R. Dronskowski, *J. Am. Chem. Soc.*, **132**, 2421–2429 (2010).
19) S. Wang, H. Ge, S. Sun, J. Zhang, F. Liu, X. Wen, X. Yu, L. Wang, Y. Zhang, H. Xu, J. C. Neuefeind, Z. Qin, C. Chen, C. Jin, Y. Li, D. He and Y. Zhao, *J. Am. Chem. Soc.*, **137**, 4815–4822 (2015).
20) K. Niwa, T. Terabe, K. Suzuki, Y. Shirako and M. Hasegawa, *J. Appl. Phys.*, **119**, 065901 (2016).
21) C. Tassel, Y. Goto, D. Watabe, Y. Tang, H. Lu, Y. Kuno, F. Takeiri, T. Yamamoto, C. M. Brown, J. Hester, Y. Kobayashi and H. Kageyama, *Angew. Chem., Int. Edit.*, **55**, 9667–9670 (2016).
22) Y. Kuno, C. Tassel, K. Fujita, D. Batuk, A. M. Abakumov, K. Shitara, A. Kuwabara, H. Moriwake, D. Watabe, C. Ritter, C. M. Brown, T. Yamamoto, F. Takeiri, R. Abe, Y. Kobayashi, K. Tanaka and H. Kageyama, *J. Am. Chem. Soc.*, **138**, 15950–15955 (2016).
23) H. Yamane and F. J. DiSalvo, *J. Solid State Chem.*, **119**, 375–379 (1995).
24) H. Yamane, M. Shimada, S. J. Clarke and F. J. DiSalvo, *Chem. Mater.*, **9**, 413–416 (1997).
25) T. Yamada, M. Imanishi, K. Nakamura, K. Murakami, H. Imabayashi, D. Matsuo, M. Honjo, M. Maruyama, M. Imade, M. Yoshimura and Y. Mori, *Appl. Phys. Express*, **9**, 071002 (2016).
26) R. Dwiliński, A. Wysmołek, J. Baranowski, M. Kamińska, R. Doradziński, J. Garczyński, L. Sierzputowski and H. Jacobs, *Acta Phys. Pol. A*, **88**, 833–836 (1995).
27) J. Li, T. Watanabe, N. Sakamoto, H. Wada, T. Setoyama and M. Yoshimura, *Chem. Mater.*, **20**, 2095–2105 (2008).
28) S. Shimada and T. Kataoka, *J. Am. Ceram. Soc.*, **84**, 2442–2444 (2001).
29) X. Piao, T. Horikawa, H. Hanzawa and K.-i. Machida, *Chem. Lett.*, **35**, 334–335 (2006).
30) A. Miura and S. Shimada, *Mater. Res. Bull.*, **41**, 1775–1782 (2006).
31) A. Miura, S. Shimada and T. Sekiguchi, *J. Cryst. Growth*, **299**, 22–27 (2007).
32) S. Shimada, Y. Miura, A. Miura and T. Sekiguchi, *Cryst. Growth Des.*, **7**, 1251–1255 (2007).
33) A. Miura, S. Shimada, T. Sekiguchi, M. Yokoyama and B. Mizobuchi, *J. Cryst. Growth*, **310**, 530–535 (2008).
34) S. H. Elder, L. H. Doerrer, F. J. Disalvo, J. B. Parise, D. Guyomard and J. M. Tarascon, *Chem. Mater.*, **4**, 928–937 (1992).
35) S. Kikkawa, K. Nagasaka, T. Takeda, M. Bailey, T. Sakurai and Y. Miyamoto, *J. Solid State Chem.*, **180**, 1984–1989 (2007).
36) H. Schilling, A. Stork, E. Irran, H. Wolff, T. Bredow, R. Dronskowski and M. Lerch, *Angew. Chem., Int. Ed.*, **46**, 2931–2934 (2007).
37) S. G. Ebbinghaus, H.-P. Abicht, R. Dronskowski, T. Müller, A. Reller and A. Weidenkaff, *Prog. Solid State Chem.*, **37**, 173–205 (2009).
38) M. Yang and F. J. DiSalvo, *Chem. Mater.*, **24**, 4406–4409 (2012).
39) Y. Masubuchi, *J. Ceram. Soc. Jpn.*, **121**, 142–149 (2013).
40) K. Kawashima, M. Hojamberdiev, H. Wagata, M. Nakayama, K. Yubuta, S. Oishi, K. Domen and K. Teshima, *Catal. Sci. Technol.*, **6**, 5389–5396 (2016).
41) R. Mikita, T. Aharen, T. Yamamoto, F. Takeiri, T. Ya, W. Yoshimune, K. Fujita, S. Yoshida, K. Tanaka, D. Batuk, A. M. Abakumov, C. M. Brown, Y. Kobayashi and H. Kageyama, *J. Am. Chem. Soc.*, **138**, 3211–3217 (2016).
42) A. Hellwig and A. Hendry, *J. Mater. Sci.*, **29**, 4686–4693 (1994).
43) K. J. Rao, B. Vaidhyanathan, M. Ganguli and P. A. Ramakrishnan, *Chem. Mater.*, **11**, 882–895 (1999).
44) H. J. Kitchen, S. R. Vallance, J. L. Kennedy, N. Tapia-Ruiz, L. Carassiti, A. Harrison, A. G. Whittaker, T. D. Drysdale, S. W. Kingman and D. H. Gregory, *Chem. Rev.*, **114**, 1170–1206 (2014).
45) C. Le Paven, R. Benzerga, A. Ferri, D. Fasquelle, V. Laur, L. Le Gendre, F. Marlec, F. Tessier, F. Cheviré, R. Desfeux, S. Saitzek, X. Castel and A. Sharaiha, *Mater. Res. Bull.*, doi:10.1016/j.materresbull.2016.11.030.
46) D. Oka, Y. Hirose, H. Kamisaka, T. Fukumura, K. Sasa, S. Ishii, H. Matsuzaki, Y. Sato, Y. Ikuhara and T. Hasegawa, *Sci. Rep.*, **4**, 4987 (2014).
47) Y. Zhang, B. Ouyang, J. Xu, G. Jia, S. Chen, R. S. Rawat and H. J. Fan, *Angew. Chem., Int. Ed.*, **55**, 8670–8674 (2016).
48) B. Mazumder and A. L. Hector, *J. Mater. Chem.*, **19**, 4673–4686 (2009).
49) Y. Xie, Y. Qian, W. Wang, S. Zhang and Y. Zhang, *Science*, **272**, 1926–1927 (1996).
50) L. Grocholl, J. Wang and E. G. Gillan, *Chem. Mater.*, **13**, 4290–4296 (2001).
51) X. Hao, M. Yu, D. Cui, X. Xu, Q. Wang and M. Jiang, *J. Cryst. Growth*, **241**, 124–128 (2002).
52) J. Choi and E. G. Gillan, *Inorg. Chem.*, **44**, 7385–7393 (2005).
53) C. Wu, T. Li, L. Lei, S. Hu, Y. Liu and Y. Xie, *New J. Chem.*, **29**, 1610–1615 (2005).
54) Y.-J. Bai, Z.-G. Liu, X.-G. Xu, D.-L. Cui, X.-P. Hao, X. Feng and Q.-L. Wang, *J. Cryst. Growth*, **241**, 189–192 (2002).
55) C.-T. Ho, K.-B. Low, R. F. Klie, K. Maeda, K. Domen, R. J. Meyer and P. T. Snee, *J. Phys. Chem. C*, **115**, 647–652 (2011).
56) Y. Setsuda, Y. Maruyama, C. Izawa and T. Watanabe, *Chem. Lett.*, doi:10.1246/cl.170267 (2017).
57) J. Choi and E. G. Gillan, *Inorg. Chem.*, **48**, 4470–4477 (2009).
58) K. Hirai, S. Isobe and K. Sada, *Sci. Rep.*, **5**, 18468 (2015).
59) A. Miura, M. Lowe, B. M. Leonard, C. V. Subban, Y. Masubuchi, S. Kikkawa, R. Dronskowski, R. G. Hennig, H. D. Abruña and F. J. DiSalvo, *J. Solid State Chem.*, **184**, 7–11 (2011).
60) A. Miura, M. Wessel and R. Dronskowski, *J. Ceram. Soc.*

Jpn., **119**, 663–666 (2011).
61) J. C. Phillips, Materials Science & Technology Ser., Bonds and Bands in Semiconductors, Academic Press (1973).
62) H. Jacobs and E. von Pinkowski, *J. Less-Common Met.*, **146**, 147–160 (1989).
63) P. E. Rauch and F. J. DiSalvo, *J. Solid State Chem.*, **100**, 160–165 (1992).
64) Y. Huang, Y. Gu, M. Zheng, Z. Xu, W. Zeng and Y. Liu, *Mater. Lett.*, **61**, 1056–1059 (2007).
65) L. Zhu, L. Chen, T. Huang, Y. Qian and Y. Gu, *J. Am. Ceram. Soc.*, **90**, 1243–1245 (2007).
66) L. Yang, H. Yu, L. Xu, Q. Ma and Y. Qian, *Dalton Trans.*, **39**, 2855–2860 (2010).
67) A. Miura, T. Takei and N. Kumada, *Cryst. Growth Des.*, **12**, 4545–4547 (2012).
68) A. Miura, T. Takei and N. Kumada, *Inorg. Chem.*, **52**, 11787–11791 (2013).
69) A. Miura, T. Takei and N. Kumada, *J. Asian Ceram. Soc.*, **2**, 326–328 (2014).
70) A. Miura, T. Takei and N. Kumada, *J. Ceram. Soc. Jpn.*, **122**, 86–88 (2014).
71) K. Guo, D. Rau, L. Toffoletti, C. Müller, U. Burkhardt, W. Schnelle, R. Niewa and U. Schwarz, *Chem. Mater.*, **24**, 4600–4606 (2012).
72) F. Tessier, A. Navrotsky, R. Niewa, A. Leineweber, H. Jacobs, S. Kikkawa, M. Takahashi, F. Kanamaru and F. J. DiSalvo, *Solid State Sci.*, **2**, 457–462 (2000).
73) A. Miura, T. Takei, N. Kumada, S. Wada, E. Magome, C. Moriyoshi and Y. Kuroiwa, *Inorg. Chem.*, **52**, 9699–9701 (2013).
74) G. Will and R. Platzbecker, *Z. Anorg. Allg. Chem.*, **627**, 2207–2210 (2001).
75) A. N. Christensen, *Acta Chem. Scand. A*, **31a**, 77–78 (1977).
76) A. L. Bowman, T. C. Wallace, J. L. Yarnell and R. G. Wenzel, *Acta Crystallogr. A*, **21**, 843 (1966).
77) J. K. Burdett and T. Hughbanks, *J. Am. Chem. Soc.*, **106**, 3101–3113 (1984).
78) R. Dronskowski and P. E. Bloechl, *J. Phys. Chem. C*, **97**, 8617–8624 (1993).
79) G. Meyer and R. Hoppe, *Z. Anorg. Allg. Chem.*, **424**, 128–132 (1976).
80) M. Kertesz and R. Hoffmann, *J. Am. Chem. Soc.*, **106**, 3453–3460 (1984).
81) A. Miura, K. Tadanaga, E. Magome, C. Moriyoshi, Y. Kuroiwa, T. Takahiro and N. Kumada, *J. Solid State Chem.*, **229**, 272–277 (2015).
82) D. S. Bem, C. M. LampeOnnerud, H. P. Olsen and H. C. zurLoye, *Inorg. Chem.*, **35**, 581–585 (1996).
83) D. S. Bem and H. C. Z. Loye, *J. Solid State Chem.*, **104**, 467–469 (1993).
84) D. S. Bem, J. D. Houmes and H. C. zur Loye, In MRS Symposium Proceeding; Covalent Ceramics II: Non-Oxides; A. R. Barron, G. S. Fischman, M. A. Fury and A. F. Hepp, Eds.; Boston (1993) pp. 153–162.
85) A. Miura, X.-D. Wen, H. Abe, G. Yau and F. J. DiSalvo, *J. Solid State Chem.*, **183**, 327–331 (2010).
86) A. Miura, T. Takei, N. Kumada, E. Magome, C. Moriyoshi and Y. Kuroiwa, *J. Alloy. Compd.*, **593**, 154–157 (2014).
87) M. Yang, A. Zakutayev, J. Vidal, X. Zhang, D. S. Ginley and F. J. DiSalvo, *Energy Environ. Sci.*, **6**, 2994–2999 (2013).
88) A. Zakutayev, C. M. Caskey, A. N. Fioretti, D. S. Ginley, J. Vidal, V. Stevanovic, E. Tea and S. Lany, *J. Phys. Chem. Lett.*, **5**, 1117–1125 (2014).
89) U. Zachwieja and H. Jacobs, *Eur. J. Sol. State Inor.*, **28**, 1055–1062 (1991).
90) A. Miura, C. Rosero-Navarro, Y. Masubuchi, M. Higuchi, S. Kikkawa and K. Tadanaga, *Angew. Chem., Int. Edit.*, **55**, 7963–7967 (2016).
91) S. Doi, A. Ishihara, S. Mitsushima, N. Kamiya and K.-i. Ota, *J. Electrochem. Soc.*, **154**, B362–B369 (2007).
92) A. Miura, M. E. Tague, J. M. Gregoire, X.-D. Wen, R. B. van Dover, H. D. Abruña and F. J. DiSalvo, *Chem. Mater.*, **22**, 3451–3456 (2010).
93) C. Pozo-Gonzalo, O. Kartachova, A. A. J. Torriero, P. C. Howlett, A. M. Glushenkov, D. M. Fabijanic, Y. Chen, S. Poissonnet and M. Forsyth, *Electrochim. Acta*, **103**, 151–160 (2013).
94) B. Cao, G. M. Veith, R. E. Diaz, J. Liu, E. A. Stach, R. R. Adzic and P. G. Khalifah, *Angew. Chem., Int. Ed.*, **52**, 10753–10757 (2013).
95) A. Seifitokaldani, M. Perrier and O. Savadogo, *J. New Mat. Elect. Syst.*, **17**, 055–065 (2014).
96) D. B. Meadowcroft, *Nature*, **226**, 847–848 (1970).
97) Y. Matsumoto, H. Yoneyama and H. Tamura, *J. Electroanal. Chem. Interfacial Electrochem.*, **83**, 237–243 (1977).
98) Y. Matsumoto, H. Yoneyama and H. Tamura, *J. Electroanal. Chem. Interfacial Electrochem.*, **79**, 319–326 (1977).
99) X. Ge, A. Sumboja, D. Wuu, T. An, B. Li, F. W. T. Goh, T. S. A. Hor, Y. Zong and Z. Liu, *ACS Catal.*, **5**, 4643–4667 (2015).
100) W. T. Hong, M. Risch, K. A. Stoerzinger, A. Grimaud, J. Suntivich and Y. Shao-Horn, *Energy Environ. Sci.*, **8**, 1404–1427 (2015).
101) J. Suntivich, H. A. Gasteiger, N. Yabuuchi, H. Nakanishi, J. B. Goodenough and Y. Shao-Horn, *Nat. Chem.*, **3**, 546–550 (2011).
102) A. Leineweber, R. Niewa, H. Jacobs and W. Kockelmann, *J. Mater. Chem.*, **10**, 2827–2834 (2000).

Akira Miura was born in Sapporo, Japan, in 1981. He received a Ph.D. in Engineering from Hokkaido University in 2007 and carried out postdoctoral research in the Department of Chemistry & Biochemistry at Cornell University and at the Institut für Anorganische Chemie at RTWH Aachen University in 2008–2010. After being appointed assistant professor at the Center for Crystal Science and Technology at Yamanashi University in 2010, he subsequently moved to the Faculty of Engineering at Hokkaido University in 2014. Dr. Miura's research interests include the synthesis and characterization of oxides, hydroxides, oxynitrides, nitrides, and oxychalcogenides for use in novel semiconductors, catalysts, superconductors, and batteries.